

## Article

# Possibilities of Mechanochemical Synthesis of Apatites with Different Ca/P Ratios

Marina V. Chaikina <sup>1</sup>, Natalia V. Bulina <sup>1,\*</sup>, Olga B. Vinokurova <sup>1</sup>, Konstantin B. Gerasimov <sup>1</sup>, Igor Yu. Prosanov <sup>1</sup>, Nikolay B. Kompankov <sup>2</sup>, Olga B. Lapina <sup>3</sup>, Evgeniy S. Papulovskiy <sup>3</sup>, Arcady V. Ishchenko <sup>3</sup> and Svetlana V. Makarova <sup>1</sup>

<sup>1</sup> Institute of Solid State Chemistry and Mechanochemistry, Siberian Branch of the Russian Academy of Sciences, Kutateladze Str. 18, 630128 Novosibirsk, Russia; d8-advance@yandex.ru (M.V.C.); bulina\_nv@mail.ru (O.B.V.); gerasimov@solid.nsc.ru (K.B.G.); prosanov@mail.ru (I.Y.P.); makarova@solid.nsc.ru (S.V.M.)

<sup>2</sup> A.V. Nikolaev Institute of Inorganic Chemistry, Siberian Branch of Russian Academy of Sciences, Lavrentyev Ave. 3, 630090 Novosibirsk, Russia; nmr124@niic.nsc.ru

<sup>3</sup> G.K. Boreskov Institute of Catalysis, Siberian Branch of Russian Academy of Sciences, Pr. Akad. Lavrentieva 5, 630090 Novosibirsk, Russia; o.b.lapina@gmail.com (O.B.L.); fyr@catalysis.ru (E.S.P.); arcady.ishchenko@gmail.com (A.V.I.)

\* Correspondence: bulina@solid.nsc.ru; Tel.: +7-383-233-24-10

**Abstract:** Apatite is widely used in medicine as a biomaterial for bone tissue restoration. Properties of apatite depend on its composition, including the Ca/P ratio. This paper shows what range of Ca/P ratio can be attained in apatite by the mechanochemical method of synthesis, providing fast formation of a single-phase product. The synthesis was carried out from a reaction mixture of CaHPO<sub>4</sub> and CaO at different Ca/P ratios in the range of 1.17–2.10. The products were studied by PXRD, FTIR and NMR spectroscopy, HRTEM, and STA. In mixtures with a low initial Ca/P ratio (1.17–1.48), directly in the mill, the formation of calcium orthophosphate with whitlockite structure containing an HPO<sub>4</sub><sup>2-</sup> group and structural water is shown for the first time. This phosphate has structure similar to that of whitlockites of hydrothermal origin and differs from high-temperature β-tricalcium phosphate that has composition Ca<sub>3</sub>(PO<sub>4</sub>)<sub>3</sub>. A series of samples of apatite was obtained with varied composition, which depends on the initial Ca/P ratio. At Ca/P < 1.67, the formation of two types of calcium-deficient apatite was documented. At Ca/P > 1.67, the existence of two types of calcium-rich apatite is confirmed.

**Keywords:** bioceramics; calcium phosphates; hydroxyapatite; calcium-deficient apatite; calcium-rich apatite; tricalcium phosphate; synthesis; mechanochemistry



**Citation:** Chaikina, M.V.; Bulina, N.V.; Vinokurova, O.B.; Gerasimov, K.B.; Prosanov, I.Y.; Kompankov, N.B.; Lapina, O.B.; Papulovskiy, E.S.; Ishchenko, A.V.; Makarova, S.V. Possibilities of Mechanochemical Synthesis of Apatites with Different Ca/P Ratios. *Ceramics* **2022**, *5*, 404–422. <https://doi.org/10.3390/ceramics5030031>

Academic Editors: Francesco Baino and Gilbert Fantozzi

Received: 15 July 2022

Accepted: 30 July 2022

Published: 3 August 2022

**Publisher's Note:** MDPI stays neutral with regard to jurisdictional claims in published maps and institutional affiliations.



**Copyright:** © 2022 by the authors. Licensee MDPI, Basel, Switzerland. This article is an open access article distributed under the terms and conditions of the Creative Commons Attribution (CC BY) license (<https://creativecommons.org/licenses/by/4.0/>).

## 1. Introduction

According to extensive literature, the prototype of the mineral component of bone and dental tissues in humans and animals is hydroxyapatite, Ca<sub>10</sub>(PO<sub>4</sub>)<sub>6</sub>(OH)<sub>2</sub> (HAp), modified with various ions at different lattice positions [1–4]. Bioapatite from hard tissues are usually poorly crystallized apatite nanocrystals [5,6] sometimes with an amorphous phase [7]. The similarity of the composition of HAp with that of the mineral component of bone has led to widespread use of synthetic HAp in medicine as a filler material for the repair of bone defects, as drug delivery systems, as an additive in toothpastes and detergents, for the production of ceramic implants or coatings on metal implants [8,9], and for the preparation of bone cements [10]. The β-form of tricalcium phosphate Ca<sub>3</sub>(PO<sub>4</sub>)<sub>2</sub> (β-TCP) having the Ca/P ratio of 1.5 is also widely employed as a material in clinical practice [11]. Sometimes, it is used in the form of a two-phase mixture with HAp, as a more easily soluble and bioavailable material [12]. Octacalcium phosphate Ca<sub>8</sub>H<sub>2</sub>(PO<sub>4</sub>)<sub>6</sub>·5H<sub>2</sub>O (OCP) having lower Ca/P ratio, namely 1.33, is also used in clinical practice for implantation into bone defects [8].

The ratio of calcium atoms to phosphorus in stoichiometric HAp is 1.67. Bioapatites are characterized by a deficiency of calcium ions and wide variation of the Ca/P ratio, which is sometimes much lower than that of stoichiometric HAp. Such apatites are usually called calcium-deficient apatite (CDAp) [1]. Compounds with  $\text{Ca/P} > 1.67$  having apatite crystal structure were named calcium-rich apatites (CRIAp) [1]. Investigations into properties of synthetic apatites with different Ca/P ratios have shown that this ratio is an important parameter that affects the properties of the material, in particular its solubility and thermal stability [8], which is crucial for practical application.

Great interest in the composition and mechanism of formation of nonstoichiometric apatites is associated with a major problem: processes of calcification in various vitally important organs, painful deposits on them in the form of nonstoichiometric compounds, and changes in the composition of bone tissues depending on various conditions and causes. Previously, it has been thought that biominerals—namely, calcified deposits on heart valves and vessels of various organs—are generated by precipitation from the surrounding fluid [1]. After that, first, a model was proposed [13], and later in vivo research revealed that apatite biominerals are formed by a precursor mechanism, where OCP precipitates first, and then it is reversibly hydrolyzed in situ to an intermediate product of the transition from OCP to HAp [14].

A substantial number of studies have been devoted to the synthesis of CDAp at various Ca/P ratios [11,12,15–18]. The authors of refs. [16,17] have synthesized CDAs with Ca/P ratio within  $1.5 \leq \text{Ca/P} \leq 1.67$  by precipitation and hydrolysis methods, respectively. The authors of paper [18] showed that hydrolysis can be used for the synthesis of CDAp with a Ca/P ratio below 1.5. Hydrolysis of a reaction product of a mixture of solutions of calcium nitrate and ammonium phosphate in the presence of hexamethylenetetramine results in the composition of the final product corresponding to the formula  $\text{Ca}_{8.5}(\text{HPO}_4)_2(\text{PO}_4)_4\text{OH}\cdot\text{H}_2\text{O}$ , i.e.,  $\text{Ca/P} = 1.416$ . Such a Ca/P ratio is observed in amorphous biological phosphates [1]. More “acidic” phosphates reaching a value of 0.5 have been synthesized by chemical precipitation in ref. [19]. In the samples with Ca/P ratios of 2.0 and 2.5, those authors registered CaO in addition to the dominant phase of HAp, indicating the impossibility of CRIAp formation by the precipitation technique.

Single-phase CRIAp samples with  $\text{Ca/P} = 1.73$  have been obtained by prolonged heating of stoichiometric HAp with  $\text{CaCO}_3$  in saturated water vapor at  $1000\text{ }^\circ\text{C}$  [20]. A series of CRIAp with  $\text{Ca/P} = 1.67\text{--}1.9$  has been synthesized from a suspension of calcium hydroxide and a solution of phosphoric acid at pH 7.5–11.5 [21]. While studying thermal decomposition of CDAp by transmission electron microscopy (TEM), the authors of ref. [22] discovered a metastable phase arising in a narrow temperature range ( $700\text{--}800\text{ }^\circ\text{C}$ ). According to energy-dispersive X-ray analysis, this metastable phase has a higher Ca/P ratio ( $>1.67$ ) than that of the HAp matrix.

We did not find research articles on the synthesis of CDAp or CRIAp by the mechanochemical method, which, under certain conditions, is a simple and fast way to obtain HAp [23]. In the mechanochemical synthesis, chemical reactions are initiated by the energy released during ball collisions and due to the action of friction forces. The released energy depends on technical characteristics of the mill, namely, kinetic energy of the balls (vial rotation speed). In this regard, the synthesis of HAp occurring directly in the milling vials is possible only in ball mills working at a high rotation speed. The higher the rotation speed of the vial, the shorter is the time needed for the HAp synthesis. The aim of the present work was to study the possible range of the Ca/P ratio in HAp forming during mechanochemical synthesis in a high-energy planetary ball mill at a rotation speed of 1800 rpm.

## 2. Materials and Methods

The initial components for the synthesis of samples were monetite  $\text{CaHPO}_4$  (of pure grade, Vekton) and freshly calcined at  $1000\text{ }^\circ\text{C}$  calcium oxide ( $\text{CaO}$ ; analytical grade, Vekton). The reagents were mixed in different ratios so that the Ca/P ratio varied from 1.17 to 2.1 (Table 1). Monetite was chosen as the initial calcium phosphate because the use of

other calcium phosphates, such as  $\text{Ca}(\text{H}_2\text{PO}_4)_2 \cdot \text{H}_2\text{O}$  and  $\text{CaHPO}_4 \cdot 2\text{H}_2\text{O}$ , is accompanied by cementation and aggregation of the mixture during activation [23]. The synthesis of the sample with  $\text{Ca}/\text{P} = 1.33$  suggested the formation of OCP having five water molecules. In this regard, the missing amount of distilled water was added to the initial reaction mixture (Table 1). Since there are no additional procedures in the synthesis other than mixing, it is obvious that all introduced elements are present in the sample, which means that the  $\text{Ca}/\text{P}$  ratio is preserved. In this regard, an elemental analysis of synthesized samples was not carried out.

**Table 1.** Reactions of mechanochemical synthesis of calcium phosphates and the intended composition of their products.

Preset Ca/P Ratio	Composition of Initial Mixture	Possible Products of Synthesis
1.17	$6\text{CaHPO}_4 + 1.02\text{CaO}$	TCP, $\text{CaHPO}_4$
1.20	$6\text{CaHPO}_4 + 1.19\text{CaO}$	TCP, $\text{CaHPO}_4$
1.21	$6\text{CaHPO}_4 + 1.23\text{CaO}$	TCP, $\text{CaHPO}_4$
1.25	$6\text{CaHPO}_4 + 1.50\text{CaO}$	TCP, $\text{CaHPO}_4$
1.33	$6\text{CaHPO}_4 + 2\text{CaO} + 3\text{H}_2\text{O}$	OCP
1.38	$6\text{CaHPO}_4 + 2.28\text{CaO}$	CDAp
1.42	$6\text{CaHPO}_4 + 2.52\text{CaO}$	CDAp
1.45	$6\text{CaHPO}_4 + 2.70\text{CaO}$	CDAp
1.48	$6\text{CaHPO}_4 + 2.88\text{CaO}$	CDAp
1.50	$6\text{CaHPO}_4 + 3.00\text{CaO}$	CDAp
1.55	$6\text{CaHPO}_4 + 3.30\text{CaO}$	CDAp
1.60	$6\text{CaHPO}_4 + 3.60\text{CaO}$	CDAp
1.67	$6\text{CaHPO}_4 + 4.00\text{CaO}$	OHAp
1.70	$6\text{CaHPO}_4 + 4.20\text{CaO}$	HAp, $\text{Ca}(\text{OH})_2$
1.80	$6\text{CaHPO}_4 + 4.80\text{CaO}$	HAp, $\text{Ca}(\text{OH})_2$
1.90	$6\text{CaHPO}_4 + 5.40\text{CaO}$	HAp, $\text{Ca}(\text{OH})_2$
2.00	$6\text{CaHPO}_4 + 6.00\text{CaO}$	HAp, $\text{Ca}(\text{OH})_2$
2.10	$6\text{CaHPO}_4 + 6.60\text{CaO}$	HAp, $\text{Ca}(\text{OH})_2$

The mechanochemical synthesis was conducted in a planetary ball mill of the AGO-2 type (ISSCM SB RAS, Russia) [24] with water-cooled vials 150 mL each at a rotation speed of 1800 rpm. The weight of the milling balls was 200 g. The weight ratio of the reaction mixture to the milling balls was 1:20. Based on ref. [23], the duration of the mechanochemical treatment was 30 min, which is sufficient for complete conversion of the initial reagents into the HAp phase. To avoid contamination of the product by the material of the balls and vials, the working zone of the vial was lined with the reaction mixture beforehand.

Products of the mechanochemical synthesis were assessed by powder X-ray diffraction (PXRD) analysis, Fourier transform infrared (FTIR) spectroscopy, TEM, nuclear magnetic resonance (NMR) spectroscopy, and simultaneous thermal analysis (STA).

The PXRD patterns were recorded on a D8 Advance powder diffractometer (Bruker, Karlsruhe, Germany) in Bragg–Brentano geometry using  $\text{CuK}\alpha$  radiation, a nickel  $\text{K}\beta$ -filter, and an ultrafast position-sensitive one-dimensional Lynx-Eye detector. The phase analysis of the compounds was carried out in the ICDD PDF-4 database (a 2011 release). The unit cell parameters, crystallite size, and the phase concentrations were determined after computation of background coefficients and sample displacement refinement by the Rietveld method in Topas 4.2 software (Bruker, Germany). The instrumental contribution was calculated by the method of fundamental parameters. The average size of the crystallites was estimated using the Lorentz convolution, which varies in  $2\Theta$  as a function of  $1/\cos(\Theta)$ . The Chebyshev polynomial of the eighth order and the  $1/x$  function were employed to describe the background.

FTIR spectra were recorded using an Infralum-801 device (Simex, Novosibirsk, Russia). The samples were prepared by the traditional KBr pellet method.

TEM and high-resolution TEM (HRTEM) images were obtained using a Themis-Z 3.1 microscope (TFS, Waltham, MA, USA) at an accelerating voltage of 200 kV. The microscope is equipped with a field emission cathode having a monochromator and with two aberration correctors. Energy-dispersive X-ray microanalysis of elemental composition of the samples was performed on a four-segment Super-X detector (with an energy resolution of  $\sim 120$  eV) in scanning dark-field mode with the construction of maps of distributions of elements by means of characteristic lines of the spectrum from each point in an analysis region. Samples for the electron-microscopic examination were dispersed by ultrasonication and deposited from alcohol on a substrate: copper perforated grids 3 mm in diameter covered with a thin carbon mesh.

Solid-state NMR experiments were conducted on a Avance III 500 spectrometer (Bruker, Karlsruhe, Germany) at a resonance frequency of 500 MHz for  $^1\text{H}$  experiments and 200 MHz for  $^{31}\text{P}$  experiments. Magic angle spinning (MAS) spectra were acquired using a 4 mm probe at sample rotation frequency 10 kHz.

STA included simultaneous detection of mass loss, differential scanning calorimetry (DSC), differential thermal analysis (DTA), and registration of the evolved gas using a mass spectrometer. STA was carried out by means of a STA 449 F1 Jupiter device (Netzsch, Lesb, Germany) equipped with a QMS 403 C Aeolos mass spectrometer. The measurements were performed in a Pt-10wt%Rh crucible under an argon-oxygen mixture (80:20) at a heating rate of  $10^\circ\text{C}/\text{min}$ .

### 3. Results

#### 3.1. PXRD

The mechanochemical synthesis of a series of samples with different Ca/P ratios was carried out in accordance with Table 1. Figure 1 shows selected PXRD patterns of the synthesized samples that have obvious differences from each other. PXRD patterns of the other samples match in appearance those presented in Figure 1. All the PXRD patterns contain clear-cut reflections indicating the presence of crystalline phases. Figure 1 shows that reflections of an HAp phase are absent in samples with Ca/P < 1.25. Nevertheless, the modeling of PXRD patterns by the Rietveld method revealed that in the region of the main reflection of HAp ( $2\theta\ 31.7^\circ$ ), there remains a certain background region, which we assigned to semiamorphous apatite. When the diffraction patterns were modeled taking into account the HAp phase with a crystallite size of less than 18 nm, reliability factors improved considerably. Given the very low degree of crystallinity of this phase, it is named as an amorphous apatite in Table 2.

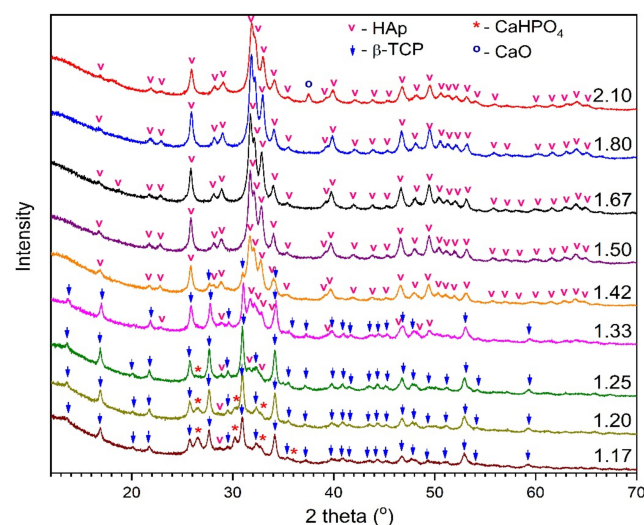


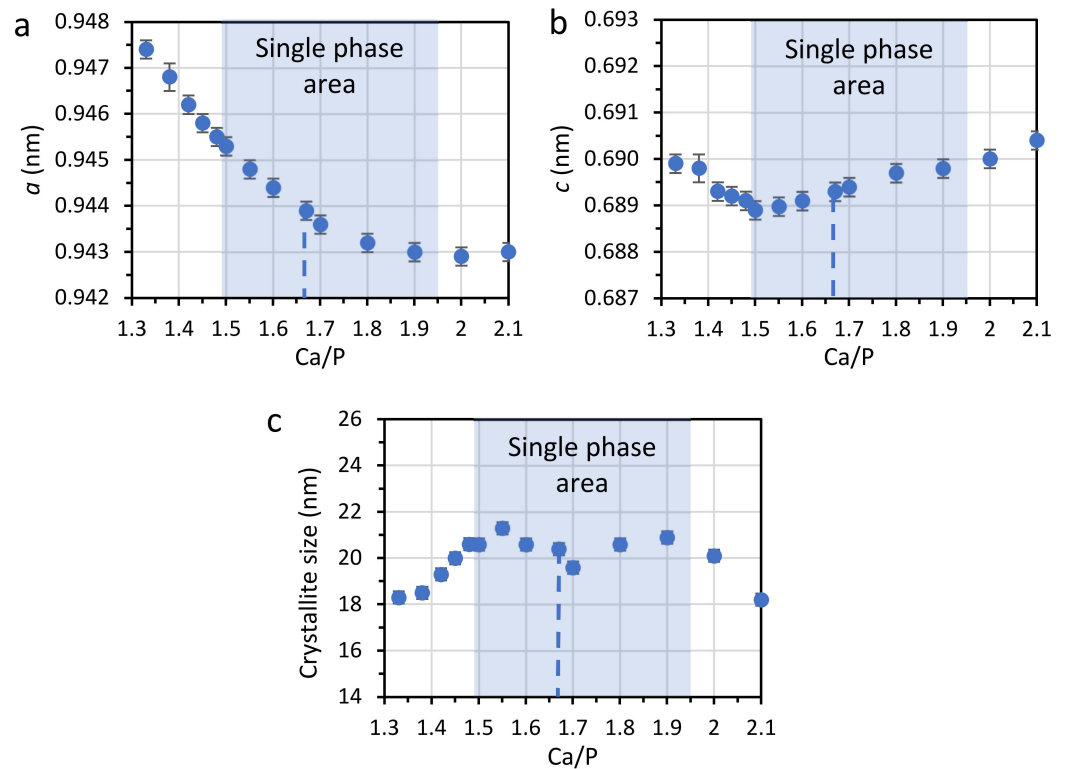
**Figure 1.** PXRD patterns of mechanochemically synthesized samples with different Ca/P ratios.

**Table 2.** Phase composition and structural data of the HAp phase in the synthesized samples.

Ca/P	Concentration (wt.%)						Structural Data for HAp			R <sub>wp</sub>
	CaHPO <sub>4</sub>	CaO	Ca(OH) <sub>2</sub>	HAp	β-TCP	Amorphous Apatite	<i>a</i> (nm)	<i>c</i> (nm)	Crystallite Size (nm)	
1.17	32	–	–	–	51	~17	0.9504	0.6911	10	5.2
1.20	24	–	–	–	62	~14	0.9504	0.6911	14	5.5
1.21	19	–	–	–	63	~18	0.9504	0.6911	15	6.1
1.25	10	–	–	24	66	–	0.9504(4)	0.6911(4)	16.1(9)	5.9
1.33	–	–	–	49	51	–	0.9474(2)	0.6899(2)	18.3(8)	4.5
1.38	–	–	–	49	51	–	0.9468(2)	0.6898(3)	18.5(4)	5.3
1.42	–	–	–	83	17	–	0.9462(2)	0.6893(2)	19.3(4)	4.9
1.45	–	–	–	95	5	–	0.9458(2)	0.6892(2)	20.0(4)	4.9
1.48	–	–	–	91	9	–	0.9455(2)	0.6891(2)	20.6(4)	4.7
1.50	–	–	–	100	–	–	0.9453(2)	0.6889(2)	20.6(2)	4.6
1.55	–	–	–	100	–	–	0.9448(2)	0.68898	21.3(2)	4.6
1.60	–	–	–	100	–	–	0.9444(2)	0.6891(1)	20.6(2)	4.5
1.67	–	–	–	100	–	–	0.9439(1)	0.6893(1)	20.4(2)	4.4
1.70	–	–	–	100	–	–	0.9436(1)	0.6894(1)	19.6(2)	4.3
1.80	–	–	–	100	–	–	0.9432(1)	0.6897(1)	20.6(2)	4.4
1.90	–	–	–	100	–	–	0.9430(1)	0.6898(1)	20.9(2)	4.3
2.00	–	1	–	99	–	–	0.9429(1)	0.6900(1)	20.1(2)	3.5
2.10	–	3	3	94	–	–	0.9430(2)	0.6904(2)	18.2(2)	3.4

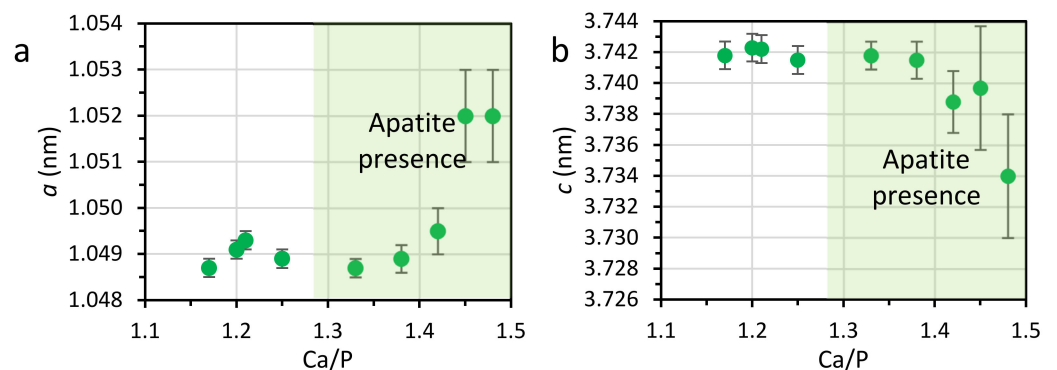
The results of phase composition analysis of the samples, as performed by the modeling of phases by the Rietveld method, are given in Table 2. This technique for analyzing diffraction patterns allows to refine crystal lattice parameters of the phases and their crystallite size, to calculate the number of phases, and to detect a minor amorphous phase. Table 2 shows that there are three Ca/P ratio ranges: single-phase (Ca/P = 1.50–1.90), two-phase (Ca/P = 1.33–1.48, 2.00), and three-phase (Ca/P = 1.25–1.17, 2.10). In the single-phase range, Ca/P = 1.5–1.9, only HAp is present. In samples with Ca/P = 1.33–1.48, in addition to HAp, a phase corresponding to β-TCP structure was registered. Reflections of this phase match card No. 040-14-2292 from the ICDD PDF-4 database. At Ca/P ≤ 1.25, the phase of the initial unreacted monetite (card No. 010-71-1759) is seen in addition to the above. In these samples, the HAp phase has a nanoscale amorphous state and a low concentration. The crystallite size is estimated to be 10–15 nm. The diffraction pattern does not contain clear-cut reflections of HAp (Figure 1), and therefore it is difficult to determine lattice parameters of this phase. At Ca/P = 2.0, in addition to HAp (card No. 010-71-1759), a phase of the initial CaO (card No. 010-82-1691) is present in the sample, and at Ca/P = 2.1, aside from the above, a Ca(OH)<sub>2</sub> phase (card No. 000-44-1481) is seen.

Figure 2a,b shows the dynamics of changes in apatite crystal lattice parameters with the increasing initial Ca/P ratio. As Ca/P goes up from 1.33 to 1.90, parameter *a* gradually decreases and stays virtually unchanged in the range of 1.9–2.10. The *c* parameter shows a different dependence, namely, it diminishes up to the ratio Ca/P = 1.5 and then begins to grow. It is noteworthy that the boundaries of the single-phase range coincide with a shift in the nature of changes in the lattice parameters: at the lower limit, dynamics of parameter *c* change, and at the upper limit, there are changes in the dynamics of parameter *a* (Figure 2a,b). The size of crystallites in the single-phase range varies between 20 and 21 nm (Figure 2c), whereas for 1.5 > Ca/P > 1.9, a decrease in this size is observed.



**Figure 2.** Dependence of the HAp lattice parameters  $a$  (a) and  $c$  (b) and crystallite size (c) on the Ca/P ratio.

Lattice parameters of the  $\beta$ -TCP phase in the range Ca/P = 1.17–1.38 do not show any pronounced dynamics (Figure 3). With a further increase in Ca/P, parameter  $a$  begins to rise while  $c$  starts to decline. It should be noted that the observed parameters' values differ substantially from those of high-temperature  $\beta$ -TCP that were obtained by the classic ceramic method; in the latter case, the material has parameters  $a = 10.427(1)$  Å and  $c = 37.456(4)$  Å [25].



**Figure 3.** Dependence of the whitlockite lattice parameters  $a$  (a) and  $c$  (b) on the Ca/P ratio.

### 3.2. FTIR Spectroscopy

Figure 4 presents FTIR spectra of synthesis products from mixtures having different initial Ca/P ratios. According to the nature of the spectrum, the data were subdivided into four ranges of changing composition of the samples. It is more convenient to start the analysis of these spectra with the identification of the spectrum of stoichiometric HAp having Ca/P = 1.67 (Figure 4d). This FTIR spectrum contains all absorption bands characteristic of stoichiometric HAp: bending  $\nu_4$  vibrations of O–P–O bonds ( $570$  and  $603$   $\text{cm}^{-1}$ ), stretching

vibrations  $\nu_1$  ( $960\text{ cm}^{-1}$ ) and  $\nu_3$  ( $1046$  and  $1088\text{ cm}^{-1}$ ) of the P–O bond, and libration ( $630\text{ cm}^{-1}$ ) and stretching vibrations ( $3572\text{ cm}^{-1}$ ) of the OH group in HAp (Figure 4d) [1]. There are weak absorption bands at  $870$ ,  $1416$ , and  $1493\text{ cm}^{-1}$  due to bending and stretching vibrations of C–O bonds of carbonate groups in apatite [1]. Mechanochemical synthesis of HAp in ambient air is usually accompanied by the incorporation of a small number of  $\text{CO}_3^{2-}$  groups into the lattice, and this number depends on the synthesis conditions [1].

In the spectra of samples with  $\text{Ca/P} > 1.67$ , positions of the absorption bands of HAp remain the same, and a small number of carbonate groups is present everywhere (Figure 4d). For samples with  $\text{Ca/P} = 1.9$  and higher, an additional band at  $3640\text{ cm}^{-1}$  appears in the spectrum, and this band's intensity grows with increasing  $\text{Ca/P}$  (Figure 4d). This band belongs to vibrations of bonds of the OH groups from calcium hydroxide  $\text{Ca(OH)}_2$ . It should be mentioned that according to our diffraction data,  $\text{Ca(OH)}_2$  is detectable only in the sample with the highest  $\text{Ca/P}$  ratio (Table 2). In this case, infrared spectroscopy turned out to be the more sensitive method.

In samples with  $\text{Ca/P}$  from  $1.60$  to  $1.50$  (Figure 4c), i.e., lower than that of stoichiometric HAp, there are no absorption bands of C–O bonds of carbonate groups. Nonetheless, in addition to the absorption bands of HAp, a wide low-intensity absorption band is seen at  $872\text{ cm}^{-1}$  (Figure 4c), indicating the presence of  $\text{HPO}_4^{2-}$  groups in the apatite lattice [1].

In the range  $1.33 \leq \text{Ca/P} \leq 1.48$ , the band of  $\text{HPO}_4^{2-}$  groups is still present (Figure 4b). A shift of absorption bands of the phosphate group to a lower-frequency region is observed, as is a change in the ratio of their intensities. The latter effect may be due to the presence of absorption bands of an additional phase ( $\beta$ -TCP), as revealed by PXRD data (Table 2). Moreover, with a decrease in  $\text{Ca/P}$ , the absorption band of the stretching vibration of the HAp hydroxyl group at  $3570\text{ cm}^{-1}$  disappears in the spectra, thus pointing to a decline of the number of hydroxyl groups.

Samples with  $1.17 \leq \text{Ca/P} \leq 1.25$  have a spectrum that is much different from that of HAp (Figure 4a). Obvious absorption bands of HAp are absent in these FTIR spectra, and hence HAp is absent in the crystalline state. According to X-ray phase analysis (Table 2), aside from amorphous HAp, these samples contain  $\beta$ -TCP and  $\text{CaHPO}_4$ . For comparison, Figure 4a shows FTIR spectra of these substances in their pure form. Readers can see that the spectra of the samples with  $\text{Ca/P} = 1.17$  and  $1.25$  are not the sum of the spectra of  $\text{CaHPO}_4$  and  $\beta$ -TCP. It can be hypothesized that these are precursors of "acidic" orthophosphates along with fragments of the structure destroyed during activation. The spectra of the analyzed samples are close in shape to the  $\beta$ -TCP spectrum; moreover, they have two bands, at  $553$  and  $606\text{ cm}^{-1}$ , matching in position. The rest of the bands are considerably shifted, implying an alteration in the immediate environment of  $\beta$ -TCP's phosphate tetrahedra. Additionally, in samples with  $\text{Ca/P} = 1.17$ – $1.25$ , there is a band at  $888\text{ cm}^{-1}$  from the  $\text{HPO}_4^{2-}$  group, which was observed at  $872\text{ cm}^{-1}$  in the samples with high  $\text{Ca/P}$  (Figure 4b) and is present in the spectrum of  $\text{CaHPO}_4$  at  $894\text{ cm}^{-1}$  (Figure 4a). The absorption band at  $1645\text{ cm}^{-1}$  belongs to adsorbed water. It must be noted that the FTIR spectra of samples with  $\text{Ca/P} = 1.17$ – $1.25$  are also similar to the spectra of amorphous phosphates [1,7].

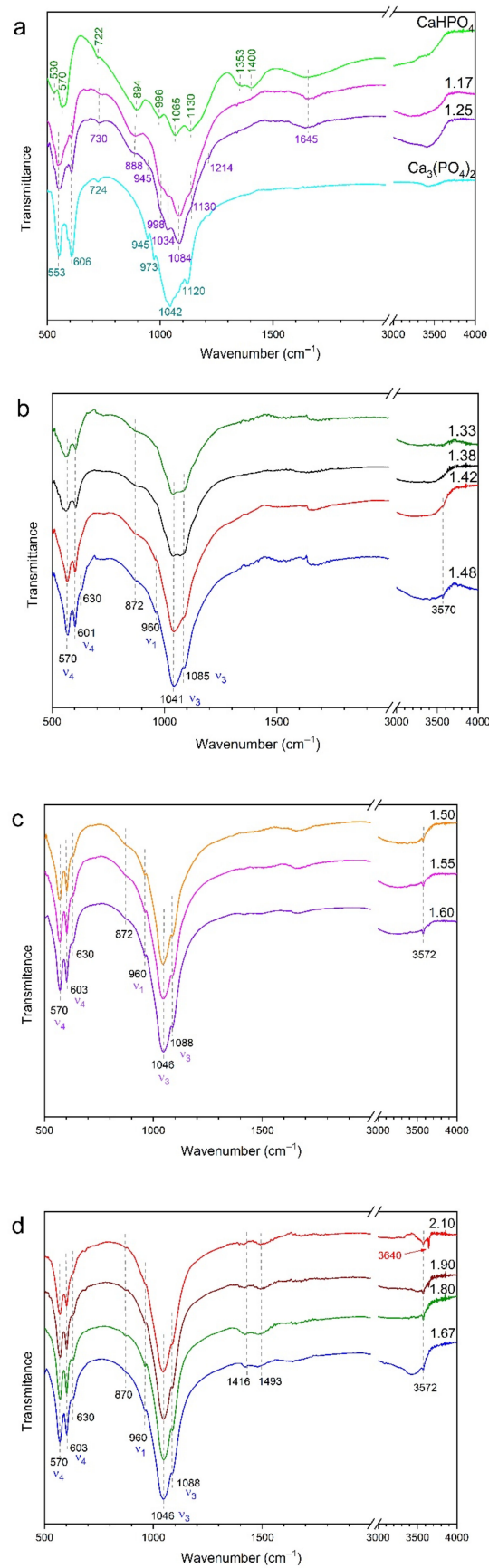


**Figure 4.** FTIR spectra of the synthesized samples with Ca/P ratios 1.17–1.25 (a), 1.33–1.48 (b), 1.50–1.6 (c), and 1.67–2.10 (d).

3.3. TEM

Figure 5 depicts electron micrographs of samples with different Ca/P ratios. All the samples are aggregates of nanoparticles ranging in size from 10 to 1000 nm. X-ray microanalysis data of the samples are shown in Figure 5. According to the results of energy-dispersive X-ray spectroscopy, in samples with low Ca/P, the distribution of elements among particles is uniform, whereas in the sample with the highest Ca/P value, different concentrations of elements are observed among particles, but the average is 2.00 (Figure 6c). The deviation of the observed Ca/P ratio from the intended ratio in the samples with Ca/P = 1.25 and 1.42 can be explained by the finding that these samples contain several phases with different Ca/P ratios, including unreacted monetite, where Ca/P = 1.00.

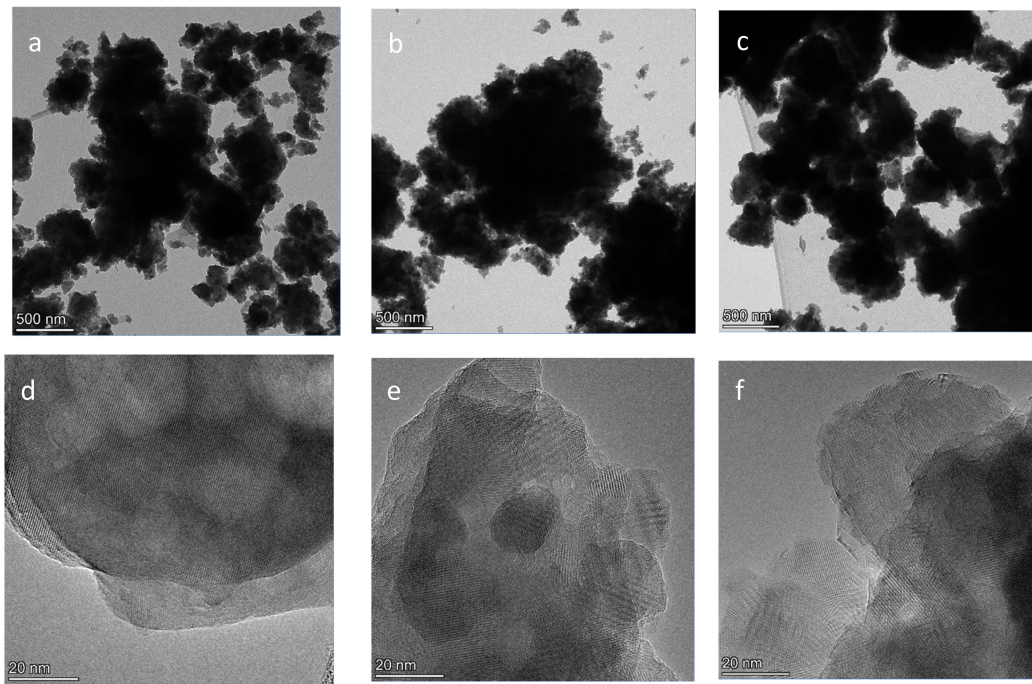


Figure 5. TEM (a–c) and HRTEM (d–f) images of samples with Ca/P ratios 1.25 (a,d), 1.42 (b,e), and 2.00 (c,f) at different magnification levels.

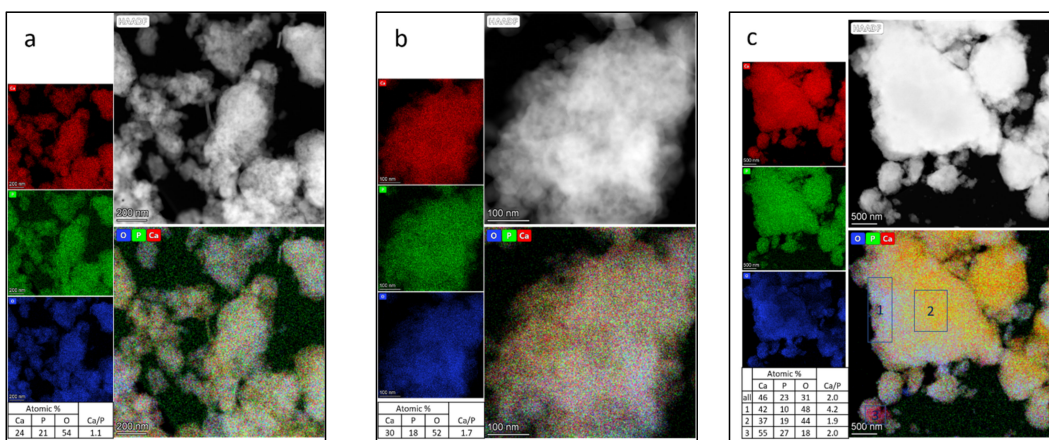
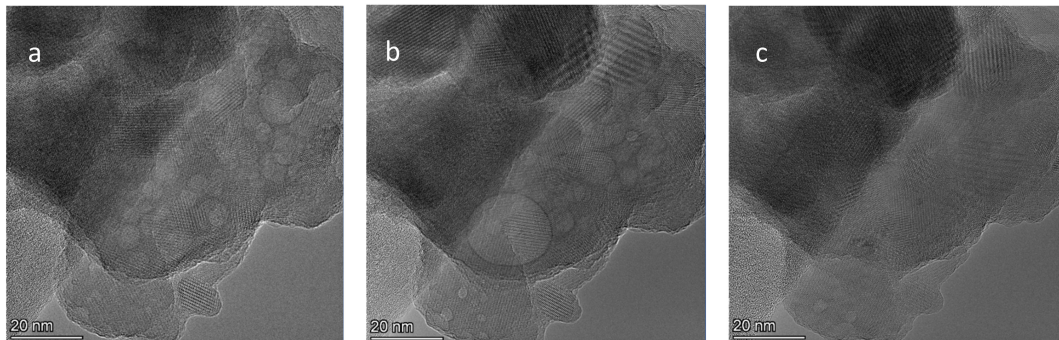


Figure 6. Distribution maps of elements across a particle in samples with Ca/P ratios 1.25 (a), 1.42 (b), and 2.00 (c).

It is worth mentioning that in the samples with Ca/P = 1.25 and 1.42, some particles contained spherical cavities in the form of bubbles. Under the influence of the electron

beam, such particles quickly transformed into monolithic ones (Figure 7, a link to a video is given in Supplementary Information).



**Figure 7.** Changes in the HRTEM image of a particle containing bubbles after 1 s (a), 30 s (b), and 60 s (c) of electron beam exposure. Ca/P = 1.42. A video showing these changes is presented as Supplementary Material.

### 3.4. NMR

$^{31}\text{P}$  and  $^1\text{H}$  MAS NMR spectra of some mechanochemically synthesized samples are given in Figure 8. The NMR parameters of the observed lines are given in Tables 3 and 4. The line fitting was carried out in accordance with literature data [26–32].

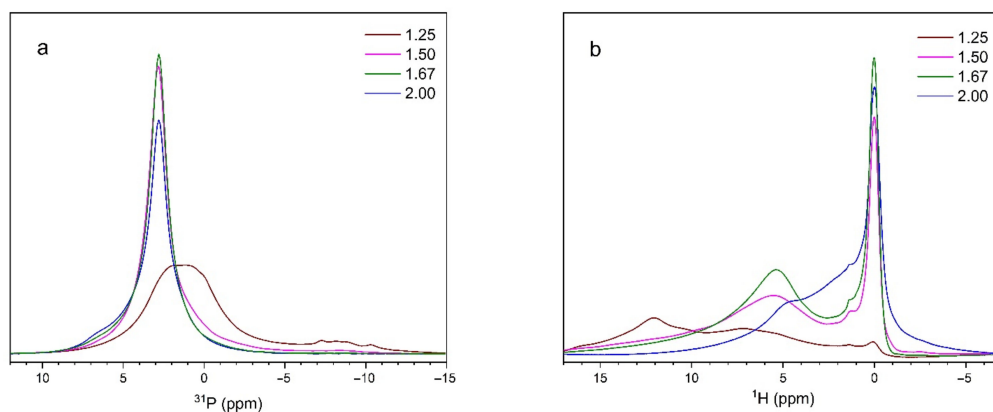


**Figure 8.**  $^{31}\text{P}$  (a) and  $^1\text{H}$  (b) MAS NMR spectra of the synthesized samples with different Ca/P ratios.

**Table 3.**  $^{31}\text{P}$  chemical shift parameters for the synthesized samples.

Ca/P		$\text{PO}_4^{3-}$	$\text{PO}_4^{3-}$ (HAp)	$\text{HPO}_4^{2-}$	$\text{Q}^{1-}$
1.25	$\delta_{iso}$ (ppm)	–	–	1.20	–7.99
	Width (Hz)	–	–	823	670
	Content	–	–	0.89	0.11
1.50	$\delta_{iso}$ (ppm)	–	2.88	–	–7.33
	Width (Hz)	–	345	–	884
	Content	–	0.96	–	0.04
1.67	$\delta_{iso}$ (ppm)	4.81	2.85	–	–
	Width (Hz)	566	273	–	–
	Content	0.11	0.89	–	–
2.00	$\delta_{iso}$ (ppm)	5.60	2.98	–	–
	Width (Hz)	466	332	–	–
	Content	0.11	0.89	–	–

**Table 4.**  $^1\text{H}$  chemical shift parameters for the synthesized samples.

Ca/P		$\text{HPO}_4^{2-}$	$\text{HPO}_4^{2-}$	$\text{H}_2\text{O}$	H-Bonded $\text{OH}^-$ (HAp)	$\text{OH}^-$ (HAp)
1.25	$\delta_{iso}$ (ppm)	16.0	12.26	6.98	1.28	0.08
	Width (Hz)	1300	1550	3400	810	317
	Content	0.08	0.33	0.54	0.03	0.02
1.50	$\delta_{iso}$ (ppm)	–	–	5.14	1.35	–0.06
	Width (Hz)	–	–	2023	170	289
	Content	–	–	0.56	0.01	0.43
1.67	$\delta_{iso}$ (ppm)	–	–	5.59	0.99	0
	Width (Hz)	–	–	2100	710	238
	Content	–	–	0.63	0.10	0.27
2.00	$\delta_{iso}$ (ppm)	–	–	4.50	1.63	0
	Width (Hz)	–	–	1693	1153	351
	Content	–	–	0.30	0.32	0.37

The signal of phosphate tetrahedra of the HAp phase ( $\delta_{iso} \approx 2.9$  ppm) is not observed in the  $^{31}\text{P}$  NMR spectrum of the sample having  $\text{Ca}/\text{P} = 1.25$ . The spectrum contains two sets of lines: a broad base with a maximum at 1.2 ppm (a superposition of at least two signals with a chemical shift of 2.5 and 0 ppm) and a broad low-intensity line at  $-8$  ppm (a superposition of at least three signals with a shift of  $-7$ ,  $-9$ , and  $-10$  ppm). According to the literature data, the peaks at  $-7.43$ ,  $-9.09$ , and  $-10.35$  ppm indicate the presence of a low amount of calcium pyrophosphate  $\text{Ca}_2\text{P}_2\text{O}_7$  [26,27]. The main phase in the sample with  $\text{Ca}/\text{P} = 1.25$  is shown in the  $^{31}\text{P}$  MAS NMR spectra as a broadened signal with a maximum at 1.2 ppm, which cannot be ascribed to  $\beta$ -TCP, as it could be proposed according to PXRD data. The  $^{31}\text{P}$  MAS NMR spectrum of  $\beta$ -TCP is extremely specific and is described by several of lines, that can be categorized into two main sets: at 5 and 0 ppm [26–29], both are absent in the sample having  $\text{Ca}/\text{P} = 1.25$  sample. The modification of  $\beta$ -TCP with a substitution of calcium with zinc or strontium leads to a major change in the spectrum; however, this kind of signal is absent [29]. A similar change in the  $^{31}\text{P}$  MAS NMR spectrum of  $\beta$ -TCP has been observed in the composite “ $\beta$ -TCP–inositol phosphate (IP6),” but the line is broader in the spectrum of this composite than in our case [31]. This substantial change in structure of  $\beta$ -TCP structure is likely to be caused by the presence of  $\text{HPO}_4^{2-}$  and a large amount of retained water exchanging with the  $\text{HPO}_4^{2-}$  group, as deduced from the  $^1\text{H}$  MAS NMR spectrum of the sample having  $\text{Ca}/\text{P} = 1.25$  (Figure 8b). Interaction of molecular water with orthophosphate groups in amorphous calcium phosphates also leads to considerable broadening of the  $^{31}\text{P}$  spectrum [33]. The signals of  $\text{HPO}_4^{2-}$  groups observed in the  $^1\text{H}$  NMR spectrum at 16.00 and 12.26 ppm can be attributed to the  $\text{CaHPO}_4$  phase [32].

A signal from phosphate tetrahedra in apatite dominates in the  $^{31}\text{P}$  NMR spectra of the samples with  $\text{Ca}/\text{P} > 1.25$  (Table 3). The narrowest signal with isotropic shift of 2.85 ppm seen in the sample with  $\text{Ca}/\text{P} = 1.67$  correspond to the structure of stoichiometric HAp. In the samples with a large and lower amount of Ca, the signal of phosphate tetrahedra in apatite is broader and shifted to low field. There is also a broadening of the signal of a hydroxyl group in the  $^1\text{H}$  spectra (Table 4).

It should be noted that the samples with  $\text{Ca}/\text{P} = 1.50$  and 1.67 contains a greater amount of retained water ( $\sim 50\%$ ; Table 4). In the sample having  $\text{Ca}/\text{P} = 2.00$ , the content of fixed water is lower: 30%; however, in the  $^1\text{H}$  spectrum, the signal at 1.63 ppm—corresponding to a hydrogen atom bonded to the hydroxyl group of HAp (Table 4)—is stronger.

## 3.5. STA

Figure 9 presents STA data for samples with  $\text{Ca}/\text{P} \leq 1.67$  and illustrates how the DSC curves become more complicated as the  $\text{Ca}/\text{P}$  ratio of the initial mixtures decreases. This finding indicates that the composition of the obtained products becomes more complicated too. In all samples, a mass loss is observed owing to the evaporation of adsorbed water, with a maximum endothermic effect between 100 and 120 °C (Figure 9a–f). Weakly bound lattice water is released at 200 °C. With a further increase in temperature during the acquisition of STA data, changes in the mass loss depend on the composition of each sample and on thermal stability of the synthesized products. Additional endothermic effects manifest themselves at lower temperatures, namely at 365–370, 430, and 650–600 °C (Figure 9a,b). These endothermic effects are due to the decomposition of unreacted monetite and of precursors of “acidic” orthophosphates with fragments of the destroyed structure during the mechanochemical synthesis. The decomposition gives rise to pyrophosphate and water.

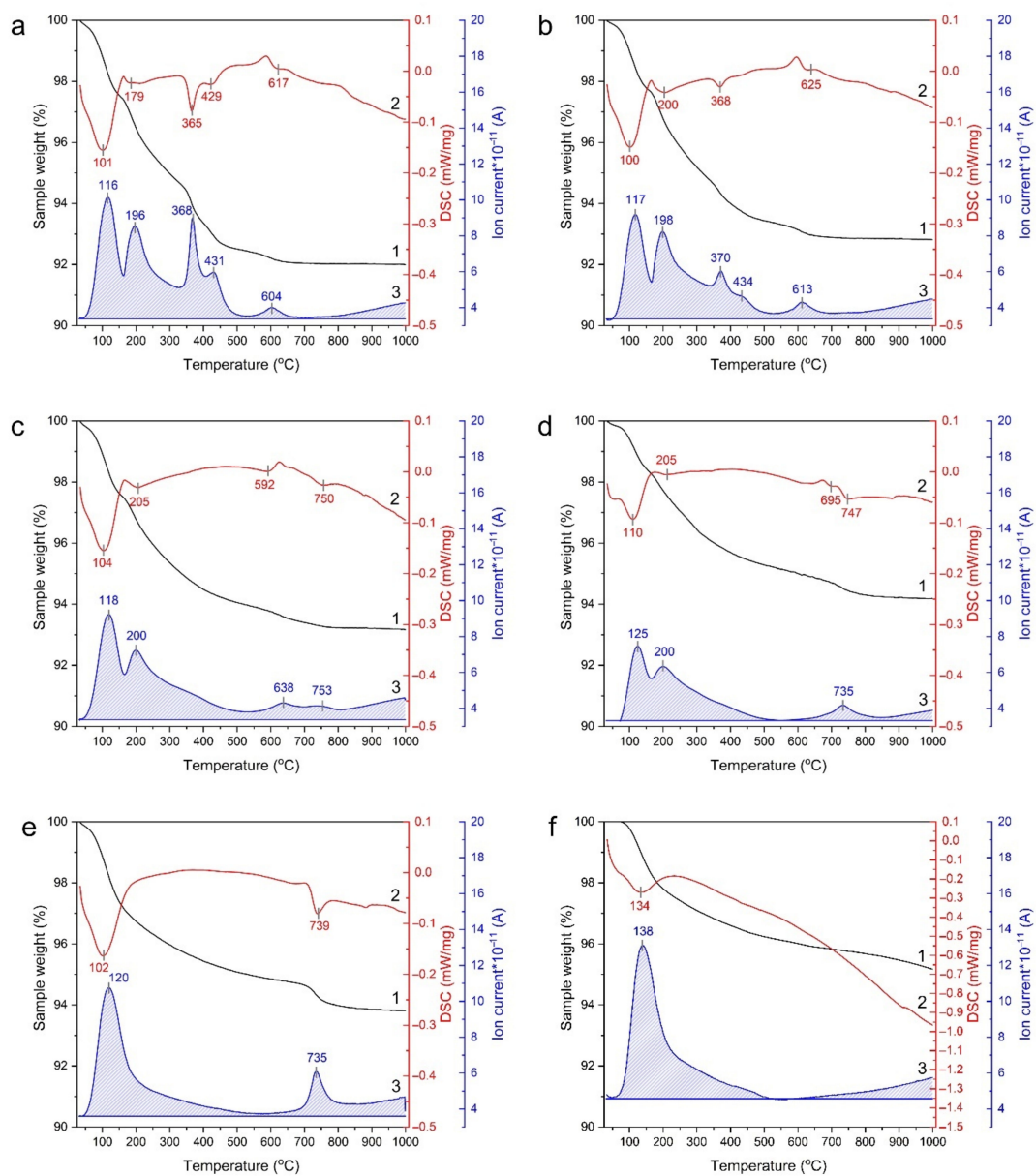
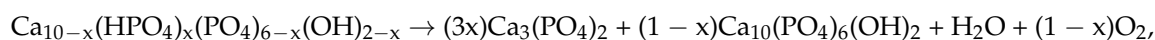


**Figure 9.** STA of samples with Ca/P ratios 1.21 (a), 1.25 (b), 1.33 (c), 1.42 (d), 1.50 (e), and 1.67 (f). 1: weight loss; 2: DSC; 3: evolution of water.

In the sample with the Ca/P ratio of 1.67, corresponding to stoichiometric HAp, the release of adsorbed water (~2%) gradually turns into a lattice water release, which lasts up to 500 °C and raises the mass loss to 3.8% (Figure 9f). The further water release observed at >700 °C is explained by HAp dehydroxylation [34].

At Ca/P = 1.50 (Figure 9e), aside from the above phenomena, an additional process takes place at 739 °C and corresponds to the decomposition of CDAP with a release of  $\beta$ -TCP, HAp, and water (Table 5 and Figure 9e) according to the reaction:



where  $x \leq 1$ .

**Table 5.** Composition of the samples after STA.

Ca/P	Concentration (wt%)		
	HAp	$\beta$ -TCP	$\text{Ca}_2\text{P}_2\text{O}_7$
1.21	–	47	53
1.25	–	56	44
1.33	–	76	24
1.42	–	90	10
1.50	8	92	–
1.67	100	–	–

After STA, the sample with Ca/P = 1.50 was biphasic (Table 5). It consisted of 92 wt% of  $\beta$ -TCP and 8 wt% of HAp. FTIR data confirmed the predominant formation of  $\beta$ -TCP in this sample (Figure 10). The spectrum shows all characteristic absorption bands consistent with Figure 3a, which presents the spectrum of a  $\beta$ -TCP standard.

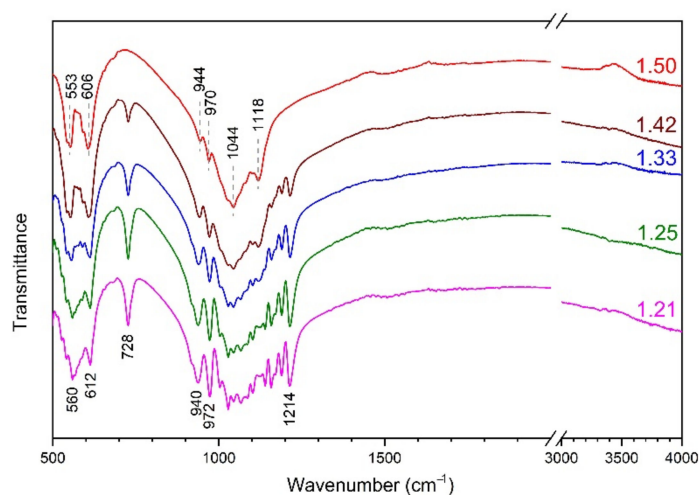


**Figure 10.** FTIR spectra of samples with different Ca/P ratios after STA.

The behavior of STA curves of the sample with Ca/P = 1.42 differs from that of the samples above by the presence of an additional endothermic effect at 205 °C because of a more intense release of lattice water (Figure 9d). After STA, in the sample with Ca/P = 1.42, HAp was no longer detectable, there was 90 wt% of  $\beta$ -TCP and 10 wt% of  $\text{Ca}_2\text{P}_2\text{O}_7$  (Table 5). The pyrophosphate is a decomposition product of more “acidic” CDAP presented in the sample with Ca/P = 1.42 as compared to the sample with Ca/P = 1.50.

In the STA curves of the sample with Ca/P = 1.33 (Figure 9c), one more endothermic process is present with a water release at 638 °C. It is worth noting that the same phases are present in this material after STA as in the sample with Ca/P = 1.42, where this endothermic effect is absent. We believe that the endothermic process at ~640 °C is also attributable to

the release of  $\beta$ -TCP, but at a lower temperature. In the sample with Ca/P = 1.33, there are probably two types of  $\beta$ -TCP precursors that decompose with the release of water at ~640 and 750 °C.

In the samples with Ca/P = 1.25 and 1.21, the water release curve clearly indicates that the observed additional endothermic effects at ~370 and ~430 °C are related to the release of water during the decomposition of unreacted monetite and of precursors of “acidic” orthophosphates with fragments of the structure destroyed during the mechanochemical synthesis (Figure 9a,b). It should also be noted that in the samples with Ca/P = 1.25 and 1.21, the formation of the  $\beta$ -TCP phase occurs in one stage and much earlier than in the above-mentioned samples (at 604–625 °C), suggesting that the composition of the  $\beta$ -TCP precursor changes. In the samples after STA, only  $\beta$ -TCP and  $\text{Ca}_2\text{P}_2\text{O}_7$  were present, as in the samples above (Table 5).

#### 4. Discussion

In this work, reactions of the synthesis of phosphates—from initial components  $\text{CaHPO}_4$  and  $\text{CaO}$  at different ratios—cover the range from Ca/P of 1.17 to 2.10. This wide range includes (i) low Ca/P ratios characteristic of CDAP, (ii) stoichiometric HAP having Ca/P = 1.67, and (iii) the range of CRIAP up to Ca/P = 2.10 (Table 1). Among these values, there are Ca/P ratios belonging to other well-studied calcium orthophosphates such as OCP (Ca/P = 1.33) and TCP (Ca/P = 1.5).

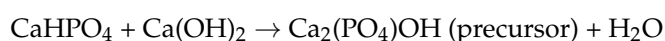
According to the obtained analytical data, the studied Ca/P range can be divided into several subranges: (1)  $\text{Ca/P} \leq 1.25$ , (2)  $1.33 \leq \text{Ca/P} \leq 1.48$ , (3)  $1.5 \leq \text{Ca/P} \leq 1.60$ , (4)  $1.67 \leq \text{Ca/P} \leq 1.90$ , and (5)  $\text{Ca/P} \geq 2$ . Each subrange is characterized by its own structural features.

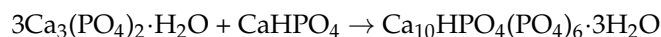
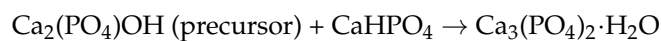
##### 4.1. Range $\text{Ca/P} \leq 1.25$

In the  $\text{Ca/P} \leq 1.25$  range, synthesis products contain unreacted monetite, amorphous apatite (most likely nuclei of CDAP and pyrophosphate), and a phase with  $\beta$ -TCP whitlockite structure; however, its lattice parameters differ considerably from those of high-temperature  $\beta$ -TCP as described above. Our FTIR and NMR spectroscopy findings also indicate some distinctive features of the  $\beta$ -TCP obtained in the current experiments. It possesses an  $\text{HPO}_4^{2-}$  group and a large amount of structural water, which is in exchange with the proton of the  $\text{HPO}_4^{2-}$  group. For this reason, samples with  $\text{Ca/P} \leq 1.25$  may begin to “come to life” and crystallize under the action of an electron beam of a microscope. The highest concentration of the whitlockite-like phase is observed in samples with Ca/P = 1.21 and 1.25 (Table 2). A further decrease or increase in Ca/P lowers its concentration. The formation of calcium phosphates with whitlockite structure but with composition more “acidic” than that of  $\beta$ -TCP is quite possible, because in our case, an excess of  $\text{CaHPO}_4$  is observed in the initial mixture.

The structure similar to whitlockite  $\beta$ -TCP and containing an “acidic” group is present in a variety of natural and synthetic compounds. Such natural minerals as calcium whitlockite  $\text{Ca}_{18.19}(\text{Mg}_{1.17}\text{Fe}_{0.63})\text{H}_{1.62}(\text{PO}_4)_{14}$  [35] and strontium whitlockite  $\text{Sr}_9\text{Mg}(\text{PO}_3\text{OH})(\text{PO}_4)_6$  [36] have been found. Calcification sites in various human and animal organs also have whitlockite structure [35]. Proton-bearing whitlockites  $\text{Ca}_{18}\text{Mn}_2\text{H}_2(\text{PO}_4)_{14}$  [37],  $\text{Ca}_{18}\text{Mg}_2\text{H}_2(\text{PO}_4)_{14}$  [35], and  $\text{Ca}_9(\text{Fe}_{0.63}\text{Mg}_{0.37})\text{H}_{0.37}(\text{PO}_4)_7$  [38] have been synthesized by the hydrothermal method. All the compounds listed in this paragraph have a PXRD pattern identical to that of high-temperature whitlockite  $\beta$ -TCP and a Ca/P ratio of <1.5.

It can be theorized that under our conditions, a mixture of  $\text{CaO}$  and  $\text{CaHPO}_4$  with an excess of the latter forms proton-containing whitlockite with the possible chemical formula  $\text{Ca}_{10}(\text{PO}_3\text{OH})(\text{PO}_4)_6$ . The interaction of the reagents involves several stages featuring intermediate products—precursors, and then the proton-containing whitlockite comes into being:





The formula  $\text{Ca}_{10}(\text{HPO}_4)(\text{PO}_4)_6$  is similar to that of the CDAP that is devoid of a hydroxyl group. The Ca/P ratio in this compound is 1.428, which can be considered as the highest possible substitution of calcium with a proton and the limit of the existence of CDAP transitioning into proton-containing whitlockite.

It was quite unexpected for us to obtain whitlockite-like structure by the mechanochemical method directly in the mill. It is known that  $\beta$ -TCP is a high-temperature form of calcium phosphate and emerges after heat treatment of a mixture of reagents with Ca/P = 1.50 at 650–750 °C [39,40]. A question arises: how can a high-temperature compound form during mechanochemical synthesis at the moderate temperature? According to literature data [41], under certain conditions of mechanochemical synthesis in powerful planetary ball mills, locally, at the contact point of the balls, the temperature can go up to 600 °C and higher. It is also known that during mechanochemical synthesis, conditions may arise where interactions of the components in the reaction mixture resemble hydrothermal ones [42], and not only high temperature but also high pressure is possible. In that detailed review, the author explains by which processes the high temperature and pressure necessary for the initiation of hydrothermal processes can be reached under the action of mechanical impulses arising in powerful planetary ball mills in solid matter–water systems. Furthermore, experimental data are presented where using several silicates as an example, products of mechanochemical synthesis have been compared with the products obtained in autoclaves. It was demonstrated above that proton-containing whitlockites can form under the conditions of hydrothermal synthesis; therefore, they can also form during mechanochemical synthesis. It is possible that it is hydrothermal processes that underlie the formation of the compound with whitlockite structure during the mechanochemical synthesis of nonstoichiometric calcium phosphates from mixtures having a low initial Ca/P ratio. The presence of  $\text{HPO}_4^{2-}$  groups and of the considerable amount of water in the lattice of these calcium phosphates testifies in favor of the hydrothermal genesis of the detected phase possessing whitlockite structure.

#### 4.2. Range $1.33 \leq \text{Ca/P} \leq 1.48$

With a further increase in the Ca/P ratio, starting reagent  $\text{CaHPO}_4$  is no longer observed among the synthesis products. In the range  $1.33 \leq \text{Ca/P} \leq 1.48$ , the whitlockite-like phase is present, and distinct reflections of an apatite phase appear (Figure 1). As Ca/P goes up, the concentration of the whitlockite phase declines (Table 2), while its crystal lattice parameters begin to deviate even more from those of stoichiometric  $\beta$ -TCP (Figure 3). It is not possible to elucidate the structure of the whitlockite formed under our conditions of mechanochemical synthesis because it is not monophasic, and its concentration diminishes with increasing Ca/P. Crystal lattice parameters of the apatite phase change too (Figure 2). A decrease in these parameters is seen, accompanied by a strong rise of this phase's concentration and by crystallite growth (Figure 2, Table 2). The presence of an absorption band of the  $\text{HPO}_4^{2-}$  group in the FTIR spectra suggests that these are CDAPs. STA findings indicate that they contain a large amount of structural water (Figure 9c,d).

There is no evidence of the presence of OCP having a ratio of Ca/P = 1.33 in the sample with the corresponding Ca/P; thus, it can be concluded that OCP is not formed by this method of mechanochemical synthesis.

#### 4.3. Range $1.50 \leq \text{Ca/P} \leq 1.60$

In this range, only the apatite phase is present among the products of the mechanochemical synthesis (Table 2), which is CDAP. The presence of the  $\text{HPO}_4^{2-}$  group is confirmed by FTIR spectroscopy. The ratio of adsorbed to lattice water increases (Figure 9f). Signals from phosphate tetrahedra and hydroxyl groups in apatites are visible in the  $^{31}\text{P}$  and  $^1\text{H}$  NMR spectra (Tables 3 and 4). Judging by the change in lattice parameters, the samples of

CDAp in this range of Ca/P ratios have varied composition approaching stoichiometric HAp. Furthermore, this composition differs from that of samples with Ca/P < 1.5 because the dynamics of parameter *c* change their direction in this range (Figure 2b). Possible composition of the CDAp within this range is  $\text{Ca}_{10-x}(\text{HPO}_4)_x(\text{PO}_4)_{6-x}(\text{OH})_{2-x}$ , where  $x \leq 1$ . The calcium deficiency is compensated by the hydrogen from the  $\text{HPO}_4^{2-}$  group, and the electroneutrality of the compound is ensured by vacancies of OH groups.

It should be pointed out that  $\beta$ -TCP, which has a Ca/P value of 1.5, was not found in the sample with the above-mentioned Ca/P ratio. In our case, the formation of proton-containing  $\beta$ -TCP was documented in mixtures with a Ca/P ratio much lower than that of  $\beta$ -TCP. At Ca/P = 1.5, only CDAp is observed as the mechanochemical-synthesis product, which blocks the formation of  $\beta$ -TCP. This result is explained by the finding that the formation of apatite structure is thermodynamically more favorable than the formation of  $\beta$ -TCP: Gibbs free energy ( $\Delta G^{\text{CDAP}}$ ) of the formation of CDAp is  $-11\,980$  kJ/mol, whereas for  $\beta$ -TCP,  $\Delta G^{\beta\text{-TCP}} = -3889$  kJ/mol. The composition of CDAp at Ca/P = 1.5 matches the formula  $\text{Ca}_9\text{HPO}_4(\text{PO}_4)_5(\text{OH})$ .

With a further decrease in the concentration of the calcium cation, i.e., with a decrease in the Ca/P ratio in apatite, the number of OH groups will be less than one (in terms of electroneutrality). In this context, the crystal lattice of CDAp will contain unit cells in which only OH group vacancies (an empty hydroxyl channel) are contained on the *c*-axis. The local excess of the positive charge should lead to a rearrangement of the structure into a “channel-less” variant; evidently for this reason, in samples with Ca/P < 1.5, a second phase separates out, which has a lower Ca/P ratio than that of  $\text{Ca}_9\text{HPO}_4(\text{PO}_4)_5(\text{OH})$  (Table 2). A similar situation of forced phase transformations in the presence of more than one vacancy per unit cell has been reported for silicate-substituted apatites, where the excess charge of the silicate anion is compensated by the emergence of a vacancy of the hydroxyl group [43]. On the other hand, a high local concentration of vacancies in CDAp can be filled with water molecules and thereby raise the *c* parameter, as observed here in the range of Ca/P < 1.5 (Figure 2b) and in agreement with the STA data (Figure 9c,d). The authors of [44] have demonstrated that CDAp with Ca/P = 1.32–1.48 can be obtained by the precipitation method.

Single-phase samples synthesized by reactions with Ca/P = 1.5–1.6 had apatite structure with varying crystal lattice parameters (Table 2).

#### 4.4. Range $1.67 \leq \text{Ca/P} < 1.90$

The formation of single-phase samples with HAp structure is observed in this range (Table 2). The first sample with Ca/P = 1.67 is HAp with a stoichiometric Ca/P value. This sample contains an adsorbed and lattice water (Figure 9f) and a negligible quantity of the carbonate ion absorbed from ambient air during the synthesis (Figure 4d). NMR data show that the signals from phosphate tetrahedra and hydroxyl groups become narrowed, indicating that the environment became more symmetrical. At the same time, in the  $^1\text{H}$  spectrum, an additional signal appears that can be explained by the exchange between the molecules of adsorbed water and the hydroxyl group of HAp.

With a further increase in Ca/P, the amount of carbonate does not rise (Figure 4d). Nonetheless, lattice parameter *a* for HAp continues to decrease, while parameter *c* keeps going up (Figure 2a,b), implying a continued change in the HAp composition. Obviously, due to the high defectiveness of the formed HAp, an increase in Ca/P above 1.67 is possible, and CRIAp arises in this range with the accommodation of excess calcium as an interstitial impurity atom.

#### 4.5. Range $\text{Ca/P} > 1.90$

The samples of this range manifested the presence of calcium hydroxide and oxide, which is a sign of excess calcium in the system. Accordingly, a further increase in calcium concentration in the apatite lattice generated by the mechanochemical synthesis is impossible; however, lattice parameter *c* of the apatite phase continues to grow in this

range (Figure 2b), while a stops diminishing. Consequently, another type of CRIAp is detectable in this range: CRIAp II. The existence of CRIAp is also supported by the data of energy-dispersive X-ray spectroscopy presented in Figure 6c. Stand-alone particles of the sample with  $\text{Ca/P} = 2.0$  had a  $\text{Ca/P}$  ratio close to or equal to the intended one.

NMR signals of phosphate tetrahedra and hydroxyl groups in apatite show a broadening (Tables 3 and 4), indicating a worsening of the symmetry of the nearest environment. This is probably caused by an increase in the number of hydrogen bonds.

Since CaO particles, which always have a hydroxide shell in the presence of water molecules, are present in this range, we can assume that this entire range is triphasic.

## 5. Conclusions

Calcium phosphates were synthesized by the mechanochemical method from mixtures of  $\text{CaHPO}_4$  and CaO with a wide range of initial  $\text{Ca/P}$  ratios: 1.17 to 2.10. For the first time, the formation of a phase possessing whitlockite structure was documented directly in a ball mill in samples with a low initial  $\text{Ca/P}$  ratio, 1.17–1.25. This phase contains an  $\text{HPO}_4^{2-}$  group and an appreciable amount of structural water. In composition and structure, the identified phase is close to whitlockites synthesized by the hydrothermal method. A hypothesis is advanced that under the conditions of “soft mechanochemical synthesis” in the planetary ball mill, the detected proton-containing whitlockite phase is produced under hydrothermal-like conditions.

A scheme is proposed for several stages of interactions between the components ( $\text{CaHPO}_4$  and CaO), where at a low  $\text{Ca/P}$  ratio of 1.17–1.25 and an excess of  $\text{CaHPO}_4$ , whitlockite  $\text{Ca}_{10}\text{HPO}_4(\text{PO}_4)_6$  forms via intermediate products under the hydrothermal conditions. The  $\text{Ca/P}$  ratio in this compound is 1.428, which can be considered the lowest  $\text{Ca/P}$  ratio and the highest substitution of calcium by protons, thereby defining the limit of the existence of CDaps transitioning into proton-containing whitlockite.

It was established that in the range  $1.33 \leq \text{Ca/P} \leq 2.10$ , a continuous series of apatites of varied composition is produced. On the basis of the initial  $\text{Ca/P}$  ratio, several sets of apatites with characteristic features can be distinguished (Figure 11). CDap of type I was registered in the range  $1.33 \leq \text{Ca/P} \leq 1.48$ . This range is biphasic. Upon transition to the single-phase range ( $1.5 \leq \text{Ca/P} < 1.67$ ), the structure of CDap alters, CDap II comes into being, which differs from CDap I by the absence of structurally bound water. Stoichiometric HAp forms at  $\text{Ca/P} = 1.67$ . Next comes the range of CRIAp of type I ( $1.5 < \text{Ca/P} \leq 1.80$ ), which transforms at  $\text{Ca/P} > 1.8$  into CRIAp II. The existence of two types of CRIAp is proposed based on the dynamics of changes in their crystal lattice parameters.

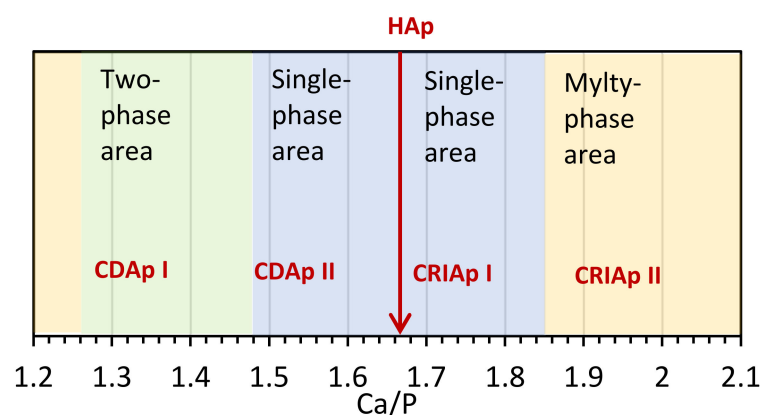


**Figure 11.** An outline of ranges of existence of the apatites produced by the mechanochemical method of synthesis.

**Supplementary Materials:** The following supporting information can be downloaded at: <https://www.mdpi.com/article/10.3390/ceramics5030031/s1>, Video S1: Video S1.avi.

**Author Contributions:** Conceptualization, M.V.C.; funding acquisition, N.V.B.; investigation, S.V.M., I.Y.P., N.B.K., A.V.I., E.S.P., K.B.G. and O.B.V.; data curation, N.V.B.; methodology, N.V.B. and M.V.C.; writing—original draft preparation, M.V.C.; writing—review and editing, N.V.B. and O.B.L. All authors have read and agreed to the published version of the manuscript.

**Funding:** This research was carried out within a state assignment to the Institute of Solid State Chemistry and Mechanochemistry SB RAS (project No. 121032500064-8).

**Institutional Review Board Statement:** Not applicable.

**Informed Consent Statement:** Not applicable.

**Data Availability Statement:** The raw/processed data required to reproduce these results are included in the Materials and Methods section.

**Acknowledgments:** The TEM analysis was conducted on the equipment of the multi-access center National Center of Catalyst Research (Novosibirsk, Russia).

**Conflicts of Interest:** The authors declare no conflict of interest. The funders had no role in the design of the study; in the collection, analyses, or interpretation of the data; in the writing of the manuscript, or in the decision to publish the results.

## References

1. Elliott, J.C. *Structure and Chemistry of Apatite and Other Calcium Orthophosphates*; Studies in Inorganic Chemistry; Elsevier: Amsterdam, The Netherlands, 1994; pp. 1–404; ISBN 0-444-81582-1.
2. Pataquiva-Mateus, A.Y.; Ferraz, M.P.; Monteiro, F.J. Nanoparticles of hydroxyapatite: Preparation, characterization and cellular approach—An Overview. *Mutis* **2013**, *3*, 43–57. [[CrossRef](#)]
3. Ptáček, P. (Ed.) Synthetic Phase with the Structure of Apatite. In *Chemistry: Apatites and their Synthetic Analogues—Synthesis, Structure, Properties and Applications*; InTech: Rijeka, Croatia, 2016; pp. 177–244. ISBN 978-953-51-2265-4. [[CrossRef](#)]
4. Turon, P.; del Valle, L.J.; Alemán, C.; Puiggali, J. Biodegradable and Biocompatible Systems Based on Hydroxyapatite Nanoparticles. *Appl. Sci.* **2017**, *7*, 60. [[CrossRef](#)]
5. Suchanek, W.; Yoshimura, M. Processing and properties of hydroxyapatite-based biomaterials for use as hard tissue replacement implants. *J. Mater. Res.* **1998**, *13*, 94–117. [[CrossRef](#)]
6. Liu, Q.; Huang, S.; Matinlinna, J.P.; Chen, Z.; Pan, H. Insight into Biological Apatite: Physicochemical Properties and Preparation Approaches. *BioMed Res. Int.* **2013**, *2013*, 929748. [[CrossRef](#)] [[PubMed](#)]
7. Combes, C.; Rey, C. Amorphous calcium phosphates: Synthesis, properties and uses in biomaterials. *Acta Biomater.* **2010**, *6*, 3362–3378. [[CrossRef](#)] [[PubMed](#)]
8. Dorozhkin, S.V. Calcium orthophosphates (CaPO<sub>4</sub>): Occurrence and properties. *Prog. Biomater.* **2016**, *5*, 9–70. [[CrossRef](#)] [[PubMed](#)]
9. Mucalo, M. *Hydroxyapatite (HAp) for Biomedical Applications*; Woodhead Publishing Limited: Waltham, MA, USA, 2015; pp. 1–364; ISBN 978-1-78242-033-0. [[CrossRef](#)]
10. Kenny, S.M.; Buggy, M. Bone cements and fillers: A review. *J. Mater. Sci. Mater. Med.* **2003**, *14*, 923–938. [[CrossRef](#)]
11. Gibson, I.R.; Rehman, I.; Best, S.M.; Bonfield, W. Characterization of the transformation from calcium-deficient apatite to  $\beta$ -tricalcium phosphate. *J. Mater. Sci. Mater. Med.* **2000**, *11*, 799–804. [[CrossRef](#)]
12. Ghosh, R.; Sarkar, R. Synthesis and characterization of sintered beta-tricalcium phosphate: A comparative study on the effect of preparation route. *Mater. Sci. Eng. C* **2016**, *67*, 345–352. [[CrossRef](#)]
13. Brown, W.E.; Eidelman, N.; Tomazic, B. Octacalcium phosphate as a precursor in biomineral formation. *Adv. Dent. Res.* **1987**, *1*, 306–313. [[CrossRef](#)]
14. Tung, M.S.; Brown, W.E. The role of octacalcium phosphate in subcutaneous heterotopic calcification. *Calcif. Tissue Int.* **1985**, *37*, 329–331. [[CrossRef](#)]
15. Vallet-Regi, M.; Navarrete, D.A. (Eds.) Biological Apatites in Bone and Teeth. In *Nanoceramics in Clinical Use: From Materials to Applications*, 2nd ed.; Royal Society of Chemistry: London, UK, 2015; pp. 1–29; ISBN 978-1-78262-255-0. [[CrossRef](#)]
16. Massit, A.; El Yacoubi, A.; Rezzouk, A.; El Idrissi, B.C. Thermal Behavior of Mg-Doped Calcium-Deficient Apatite and Stabilization of beta Tricalcium Phosphate. *Biointerface Res. Appl. Chem.* **2020**, *10*, 6837–6845. [[CrossRef](#)]
17. Nakahira, A.; Nakata, K.; Numako, C.; Murata, H.; Matsunaga, K. Synthesis and Evaluation of Calcium-Deficient Hydroxyapatite with SiO<sub>2</sub>. *Mater. Sci. Appl.* **2011**, *2*, 1194–1198. [[CrossRef](#)]
18. Andrés-Vergés, M.; Fern, C.; Martínez-Gallego, M.; Solier, J.D.; Cachadiña, I.; Matijević, E. A new route for the synthesis of calcium-deficient hydroxyapatites with low Ca/P ratio: Both spectroscopic and electric characterization. *J. Mater. Res.* **2000**, *15*, 2526–2533. [[CrossRef](#)]

19. Ergun, C.; Evis, Z.; Webster, T.J.; Sahin, F.C. Synthesis and microstructural characterization of nano-size calcium phosphates with different stoichiometry. *Ceram. Int.* **2010**, *37*, 971–977. [[CrossRef](#)]
20. Bonel, G.; Heughebaert, J.C.; Heughebaert, M.; Lacout, J.L.; Lebugle, A. Apatite calcium orthophosphates and related compounds for biomaterials preparation. *Ann. N. Y. Acad. Sci.* **1988**, *523*, 115–130. [[CrossRef](#)]
21. Ansari, M.; Naghib, S.M.; Moztarzadeh, F.; Salati, A. Synthesis and characterization of hydroxyapatite calcium hydroxide for dental composites. *Ceramucs-Silikáty* **2011**, *55*, 123–126.
22. Tamai, M.; Nakamura, M.; Isshiki, T.; Nishio, K.; Endoh, H.; Nakahira, A. A metastable phase in thermal decomposition of Ca-deficient hydroxyapatite. *J. Mater. Sci. Mater. Med.* **2003**, *14*, 617–622. [[CrossRef](#)]
23. Chaikina, M.V.; Bulina, N.V.; Vinokurova, O.B.; Prosanov, I.Y.; Dudina, D.V. Interaction of calcium phosphates with calcium oxide or calcium hydroxide during the “soft” mechanochemical synthesis of hydroxyapatite. *Ceram. Int.* **2019**, *45*, 16927–16933. [[CrossRef](#)]
24. *Patent of Russian Federation*; №975068; Bull. Inv.: Moscow, Russia, 1982; p. 43.
25. Chaikina, M.V.; Bulina, N.V.; Vinokurova, O.B.; Prosanov, I.Y. Synthesis of Stoichiometric and Substituted  $\beta$ -Tricalciumphosphate using Mechanochemistry. *Chem. Sustain. Dev.* **2020**, *28*, 73–78. [[CrossRef](#)]
26. Sakka, S.; Bouaziz, J.; Ben, F. Mechanical Properties of Biomaterials Based on Calcium Phosphates and Bioinert Oxides for Applications in Biomedicine. In *Advances in Biomaterials Science and Biomedical Applications*; Pignatello, R., Ed.; InTech: Rijeka, Croatia, 2013; pp. 23–50. ISBN 978-953-51-1051-4. [[CrossRef](#)]
27. Trandafir, D.L.; Mirestean, C.; Turcu, R.V.F.; Frentiu, B.; Eniu, D.; Simon, S. Structural characterization of nanostructured hydroxyapatite-iron oxide composites. *Ceram. Int.* **2014**, *40*, 11071–11078. [[CrossRef](#)]
28. Legrand, A.P.; Bresson, B.; Guidoin, R.; Famery, R. Mineralization followup with the use of NMR spectroscopy and others. *J. Biomed. Mater. Res.* **2002**, *63*, 390–395. [[CrossRef](#)]
29. Boanini, E.; Gazzano, M.; Nervi, C.; Chierotti, M.R.; Rubini, K.; Gobetto, R.; Bigi, A. Strontium and Zinc Substitution in  $\beta$ -Tricalcium Phosphate: An X-ray Diffraction, Solid State NMR and ATR-FTIR Study. *J. Funct. Biomater.* **2019**, *10*, 20. [[CrossRef](#)] [[PubMed](#)]
30. Yashima, M.; Sakai, A.; Kamiyama, T.; Hoshikawa, A. Crystal structure analysis of  $\beta$ -tricalcium phosphate  $\text{Ca}_3(\text{PO}_4)_2$  by neutron powder diffraction. *J. Solid State Chem.* **2003**, *175*, 272–277. [[CrossRef](#)]
31. Konishi, T.; Yamashita, K.; Nagata, K.; Lim, P.N.; Thian, E.S.; Aizawa, M. Solid-state nuclear magnetic resonance study of setting mechanism of  $\beta$ -tricalcium phosphate-inositol phosphate composite cements. *J. Phys. Mater.* **2019**, *2*, 034007. [[CrossRef](#)]
32. Jäger, C.; Welzel, T.; Meyer-Zaika, W.; Epple, M. A solid-state NMR investigation of the structure of nanocrystalline hydroxyapatite. *Magn. Reson. Chem.* **2006**, *44*, 573–580. [[CrossRef](#)] [[PubMed](#)]
33. Mathew, R.; Gunawidjaja, P.N.; Izquierdo-Barba, I.; Jansson, K.; García, A.; Arcos, D.; Vallet-Regí, M.; Edén, M. Solid-State  $^{31}\text{P}$  and  $^1\text{H}$  NMR Investigations of Amorphous and Crystalline Calcium Phosphates Grown Biomimetically from a Mesoporous Bioactive Glass. *J. Phys. Chem. C.* **2011**, *115*, 20572–20582. [[CrossRef](#)] [[PubMed](#)]
34. Tõnsuaadu, K.; Gross, K.A.; Plūduma, L.; Veiderma, M. A review on the thermal stability of calcium apatites. *J. Therm. Anal. Calorim.* **2012**, *110*, 647–659. [[CrossRef](#)]
35. Calvo, C.; Gopal, R. The Crystal Structure of Whitlockite from the Palermo Quarry. *Am. Mineral.* **1975**, *60*, 120–133.
36. Britvin, S.N.; Pakhomovskii, Y.A.; Bogdanova, A.N.; Skiba, V.I. Strontiovitlockite,  $\text{Sr}_9\text{Mg}(\text{PO}_3\text{OH})(\text{PO}_4)_6$ , a new mineral species from the Kovdor deposit, Kola Peninsula, USSR. *Can. Mineral.* **1991**, *29*, 87–93.
37. Kostiner, E.; Rea, J.R. The crystal structure of manganese-whitlockite,  $\text{Ca}_{18}\text{Mn}_2\text{H}_2(\text{PO}_4)_{14}$ . *Acta Crystallogr. Sect. B Struct. Crystallogr. Cryst. Chem.* **1976**, *32*, 250–253. [[CrossRef](#)]
38. Deyneko, D.V.; Aksenov, S.M.; Morozov, V.A.; Stefanovich, S.Y.; Dimitrova, O.V.; Barishnikova, O.V.; Lazoryak, B.I. A new hydrogen-containing whitlockitetype phosphate  $\text{Ca}_9(\text{Fe}_{0.63}\text{Mg}_{0.37})\text{H}_{0.37}(\text{PO}_4)_7$ : Hydrothermal synthesis and structure. *Z. Kristallographie-Cryst. Mater.* **2014**, *229*, 823–830. [[CrossRef](#)]
39. Destainville, A.; Champion, E.; Bernache-Assollant, D.; Laborde, E. Synthesis, characterization and thermal behavior of apatitic tricalcium phosphate. *Mater. Chem. Phys.* **2003**, *80*, 269–277. [[CrossRef](#)]
40. Bohner, M.; Santoni, B.L.G.; Döbelin, N.  $\beta$ -tricalcium phosphate for bone substitution: Synthesis and properties. *Acta Biomater.* **2020**, *113*, 23–41. [[CrossRef](#)]
41. Kwon, Y.S.; Gerasimov, K.B.; Yoon, S.K. Ball temperatures during mechanical alloying in planetary mills. *J. Alloys Compd.* **2002**, *346*, 276–281. [[CrossRef](#)]
42. Boldyrev, V.V. Hydrothermal reactions under mechanochemical action. *Powder Technol.* **2002**, *122*, 247–254. [[CrossRef](#)]
43. Bulina, N.V.; Chaikina, M.V.; Andreev, A.S.; Lapina, O.B.; Ishchenko, A.V.; Prosanov, I.Y.; Gerasimov, K.B.; Solovyov, L.A. Mechanochemical Synthesis of  $\text{SiO}_4^{4-}$ -Substituted Hydroxyapatite, Part II—Reaction Mechanism, Structure, and Substitution Limit. *Eur. J. Inorg. Chem.* **2014**, *2014*, 4810–4825. [[CrossRef](#)]
44. Christoffersen, J.; Christoffersen, M.R.; Kibalczyk, W.; Andersen, F.A. A contribution to the understanding of the formation of calcium phosphates. *J. Cryst. Growth* **1989**, *94*, 767–777. [[CrossRef](#)]